Biomaterials Science

ROYAL SOCIETY OF CHEMISTRY

PAPER

View Article Online
View Journal | View Issue

Cite this: *Biomater. Sci.*, 2021, **9**, 6927

Enhanced clearing of *Candida* biofilms on a 3D urothelial cell *in vitro* model using lysozyme-functionalized fluconazole-loaded shellac nanoparticles†

Anheng Wang, [a] Paul J. Weldrick, [a] Leigh A. Madden [b] and Vesselin N. Paunov *[c]

Candida urinary tract biofilms are increasingly witnessed in nosocomial infections due to reduced immunity of patients and the hospital ecosystem. The indwelling devices utilized to support patients with urethral diseases that connect the unsterilized external environment with the internal environment of the patient are another significant source of urinary tract biofilm infections. Recently, nanoparticle (NP)-associated therapeutics have gained traction in a number of areas, including fighting antibiotic-resistant bacterial biofilm infection. However, most studies on nanotherapeutic delivery have only been carried out in laboratory settings rather than in clinical trials due to the lack of precise *in vitro* and *in vivo* models for testing their efficiency. Here we develop a novel biofilm-infected 3D human urothelial cell culture model to test the efficiency of nanoparticle (NP)-based antifungal therapeutics. The NPs were designed based on shellac cores, loaded with fluconazole and coated with the cationic enzyme lysozyme. Our formulation of 0.2 wt% lysozyme-coated 0.02 wt% fluconazole-loaded 0.2 wt% shellac NPs, sterically stabilised by 0.25 wt% poloxamer 407, showed an enhanced efficiency in removing *Candida albicans* biofilms formed on 3D layer of urothelial cell clusteroids. The NP formulation exhibited low toxicity to urothelial cells. This study provides a reliable *in vitro* model for *Candida* urinary tract biofilm infections, which could potentially replace animal models in the testing of such antifungal nanotechnologies. The reproducibility and availability of a well-defined biofilm-infected 3D urothelial cell culture model give valuable insights into the formation and clearing of fungal biofilms and could accelerate the clinical use of antifungal nanotherapeutics.

Received 29th June 2021,
Accepted 28th August 2021

DOI: 10.1039/d1bm01035b

rsc.li/biomaterials-science

Introduction

Urinary tract infections (UTIs) are one of the most common diseases in all age groups, consuming many medical resources.[1] UTIs are most common in women, with the lifetime incidence exceeding 40%.[2] UTIs can be divided into cystitis, pyelonephritis, and prostatitis based on the analysis of clinical symptoms and microbiological types.[3–5] The main sites of infection in these three types of urinary tract infections are the lower urinary tract, upper urinary tract, and kidney or prostate.[6]

Candida urinary tract infections are relatively rare in healthy individuals but are more likely to occur in nosocomial infections.[7] This is highly associated with the patient's reduced immunity. The hospital ecosystem also contributes to the increased rate of urinary tract infections among patients. *Candida albicans* infections account for 42 percent of hospital-acquired urinary tract infections in infants.[8] Another primary source of nosocomial infection in the urinary tract are indwelling devices that are used to support patients who have urethral diseases, such as catheters and stents.[9,10]

The relevance of biofilms to catheter-associated urinary tract infection (CAUTI) is that a foreign body, such as an indwelling urethral catheter, connecting a normally sterile, hydrated body site to the outside world will inevitably become colonized with microorganisms significantly increasing the risk of biofilm infection.[11–13] Indwelling medical devices are often colonized by bacteria or fungal cells, which are able to form an extracellular polymeric substance (EPS) to encapsulate and protect their colony. The EPS allows them to proliferate

[a]*Department of Chemistry, University of Hull, Cottingham Road, Hull, HU67RX, UK*
[b]*Department of Biomedical Sciences, University of Hull, Hull, HU67RX, UK*
[c]*Department of Chemistry, Nazarbayev University, 53 Kabanbay Batyr Avenue, Nursultan city, 010000, Kazakhstan. E-mail: vesselin.paunov@nu.edu.kz*

†Electronic supplementary information (ESI) available: Fig. S1–S5 and fluconazole nanocarrier preparation and characterization methodology. See DOI: 10.1039/d1bm01035b

and increase their adhesion to the tissue and enhance their resistance to drugs.[14,15] This unique ecosystem, called a biofilm, enhances the production of DNA, RNA, polysaccharides, and proteins by higher cell–cell interaction.[16,17] The absorption properties of the EPS to a range of molecules, including antibiotics and antifungals, and the excretion of extracellular enzymes additionally boost the colony antimicrobial resistance.[18,19]

Recently, nanotechnology-based approaches have started to gain traction for creating new antimicrobial formulations and delivery systems that are able to penetrate the EPS of biofilms and kill multidrug-resistant microbial strains.[20,21] The existing nanoparticle therapies are mainly based on inorganic substances, polymers, and various macromolecules and small molecules that have been shown to be useful in preventing the formation of biofilms.[22–25] These nanoparticles are typically manufactured by microfluidics, self-assembly, or mechanical stretching and exhibit controllable sizes, shapes, and surface properties.[26–28]

Recently, polymeric antimicrobial nanocarriers,[46–50] metal-based nanocomposites,[51–53] carbon-based nanomaterials, and dual functionalized nanoparticles have been developed into a valuable nanotechnology to enhance antimicrobial effects and revive old antibiotics.

An increasing number of nanotechnology-based antimicrobials hold promising potential against the threat of antibiotic-resistant biofilms under laboratory conditions.[24–30,58] One major issue that has dominated the nanotechnology field for many years is the lack of realistic *in vitro* testing platforms and animal models, which are essential before the clinical trial. Despite the safety and efficacy, animal models are often limited by their ethical and moral concerns. The existing *in vitro* models, such as 2D human cell culture, are too simplistic for biofilm simulation. More recently, literature has emerged that offers 3D cell culture, balancing the complexity of real organs and availability.[31,32] 3D cell cultures use microfluidics, extracellular matrix (ECM), or other devices to enhance cell-to-cell contact and produce organoid/spheroid cells with enhanced cell-to-cell signals and functionality.[33–35] These models are believed to be more advanced in simulating the *in vivo* environment, and their cell cluster sizes (200 μm or larger) make it feasible to test the effect of drugs on specific tissues. Research on this subject has been mostly limited to the fabrication of spheroids with a very low yield, which strongly inhibits its application in the biomedical area. There are different types of 3D microenvironments in the biofilm (EPS) and the urothelial clusteroids (ECM), respectively. The potential interaction between biofilm's EPS and clusteroids' ECM would depend on the maturity of the biofilm, which is obviously very important for its adhesion to the underlying tissue and the proliferation of the fungal infection. When a fungal biofilm infection occurs, they may merge, as the fungal biofilm is on the outer layer of the urothelial cells and can penetrate in between the cells in the clusteroids. This topic is worth pursuing in a separate study focused on these interactions.

Recently, Das *et al*. proposed the use of an aqueous two-phase system (ATPS) water-in-water Pickering emulsion for the high throughput production of spheroids has emerged.[36] Several researchers have reported that this unique technology could rapidly produce spheroids with considerable yields and enhanced functionality.[37,38] This opens the possibility for using a 3D urinary cell culture model to simulate the urinary fungal biofilm infection *in vitro*.

Here, we employed the cell line ECV 304, which is recognized as a mature bladder cell model with endothelial cell properties, high availability and stable phenotype, to produce 3D urinary cell clusteroid models using the ATPS based templating method.[36–38] We inoculated the 3D layer of urothelial cell clusteroids with a *Candida albicans* biofilm infection, followed by testing of the selected nano-formulation, fluconazole-loaded poloxamer 407 stabilised shellac nanoparticles, surface functionalized with lysozyme, for its efficiency in clearing the biofilm. Note that the nanotechnology used here for the treatment of the fungal biofilm could be altered to any existing models. Here we use one of our established antifungal shellac nanocarrier systems with a novel enzymatic surface functionality of lysozyme and fluconazole payload, as an example. The schematics of our experiments is summarized in Fig. 1.

There are two primary aims of this study: (i) to investigate the feasibility of the fungal infection on 3D urinary cell models and (ii) to ascertain the efficiency of the selected nanotechnology for clearing fungal biofilms on the 3D urinary cell layer. This study provides an exciting opportunity to advance the current *in vitro* models in simulating urinary tract biofilm infection. The tested nano-formulation could prove to be effective for the downstream applications of the exceeding number of nanotechnologies.

We envisage that such an antifungal nano-formulation could be used in future clinical studies for clearing fungal biofilms on the bladder and urethra walls. Biofilms on the urothelium could potentially be clinically targeted by delivering the dual functionalised nano-formulation into the bladder by the catheter system through the urethra, where after clearing of the biofilm infection it would be naturally excreted through the patient urinary tract. This nanotechnology may open the way for treating persistent fungal biofilm infections, and the 3D urinary cell model is a good way of examining its efficacy along with the testing of its biocompatibility with the cells of the urothelium.

Materials and methods

Materials

Shellac aqua solution (25 wt% aqueous suspensions) was sourced from SSB® AquaGold. The fungal species *Candida albicans* (Robin) Berkhout (ATCC MYA-2876) was obtained from the ATCC. Poloxamer 407 (P407, analytical grade) and lysozyme powder (from hen egg white), poly-L-lysine, and sodium alginate were obtained from Sigma-Aldrich, UK. Whey protein was a gift from No. 1 Supplements, Suffolk, UK. Dulbecco's modified Eagle's medium, Corning® Transwell® polyester membrane cell culture inserts (96 microwell plates),

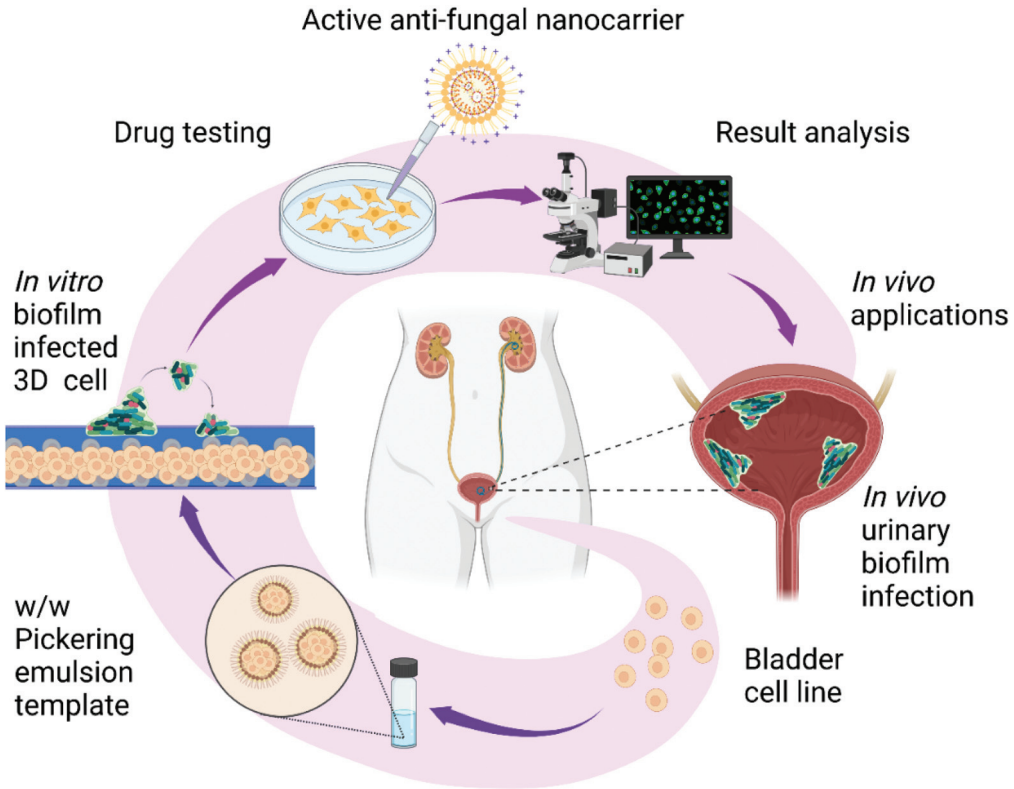

Fig. 1 Schematic illustration of the *in vitro* 3D urinary cell model for testing anti-fungal nanotechnologies. Partially created with BioRender.com.

0.25% trypsin-EDTA solutions, and Nunc cell culture 6-well plates were purchased from Thermo Fisher Scientific (UK). The RPMI 1604 medium (BE12-702F) supplemented with L-glutamine for the fungal cell culture was sourced from Lonza, Basel, Switzerland. Dextran DEX, (M.W. 500 kDa) and polyethylene oxide (PEO, M.W. 200 kDa) were purchased from Alfa Aesar, UK. Mueller–Hinton Broth (MHB) and Mueller–Hinton Agar (MHA) were sourced from Oxford, UK. The Optimal Cutting Temperature (OCT) compound was sourced from Cellpath™ OCT Embedding Matrix (Fisher scientific, Loughborough, UK). Foetal bovine serum (FBS) was purchased from Labtech, Heathfield, UK. Fluconazole (99%) was purchased from Alfa Aesar, UK. CellTiter 96® AQ ueous One Solution Cell Proliferation Assay (MTS) kit was purchased from Promega, (Madison, USA). Deionized water purified using a MilliQ water system (Millipore) was used in all experiments.

ECV 304 monolayer cell culture

The ECV 304 cell line is derived from human urinary bladder carcinoma, and also represents many features of endothelial cells. This unique feature will make them a valuable model for the study of cellular processes in the urothelium/bladder cell behaviours and the cell–cell interactions. The dual cell characteristics combined with a fast proliferation rate also make this cell line an ideal *in vitro* model for biofilm infection testing, as described below. The ECV 304 cell line was sourced from the ECACC cell collection and was cultured in DMEM medium supplemented with 10% FBS sourced from Labtech, UK. The ECV 304 cells were incubated in a T75 EasYFlask (Thermo Fisher Scientific, UK) at 37 °C under 5% CO_2 before the confluency reached 80%. The medium was discarded, and the cells were rinsed with phosphate buffered saline (PBS, Lonza, UK) twice to remove the excessive medium. The cells were passaged at a ratio of 1 : 8 using 0.25 wt% trypsin solution. The trypsinization was neutralized by adding a complete DMEM medium, and the cells were collected by centrifugation at 400*g* for 4 min.

Production of a 3D layer of ECV 304 cell clusteroids

The protocol of producing ECV 304 3D clusteroids was retouched from the method introduced by Das *et al.*[36] Briefly, the protocol is based on an ATPS, water-in-water Pickering emulsion. 22 g PEO and 11 g dextran powders were suspended in 50 mL deionized water, followed by autoclaving (121 °C, 15 min) to obtain 22 wt% PEO and 11 wt% DEX sterile solution. 11 wt% PEO was blended with an equal volume of heat-treated whey protein particle (WPP) suspension[36,37] before mixing with DMEM complete medium at a ratio of 1 : 1 to obtain 5.5 wt% PEO/DMEM/WPP solution. Similarly, a 5.5 wt% DEX solution was obtained in DMEM. The dextran phase (DEX) was used as the dispersed phase, where the ECV 304 cells were initially affiliated to and altered to a fixed cell concentration (1×10^6 mL^{-1}). The DEX and PEO phases were gently emulsified using a BD Plastipak™ syringe fitted with a

BD Microlance™ 12 needle (21G 12, internal diameter: 0.512 mm, BD Biosciences, Wokingham, UK) by 6 pumps. After the DEX/PEO w/w Pickering emulsion was fabricated, the affiliation of the cells to the DEX phase would facilitate their encapsulation in the DEX droplets. The cells were compressed to form cell clusteroids by adding PEO/DMEM solution with a higher concentration (11 wt%) to a final PEO concentration of 8 wt%. This causes a transfer of water from the DEX drops to the continuous PEO phase, which shrinks the DEX drops along with the encapsulated cells. The w/w Pickering emulsions were incubated overnight to generate clusteroids by increased cell–cell interactions. The emulsions were diluted ten-fold with a DMEM complete medium to enable the emulsion to break down and to allow sedimentation of the clusteroids by gravity. The clusteroids were then taken out and transferred to poly-L-lysine coated 6-well plates to produce a 3D layer of ECV 304 cell clusteroids. The culture was incubated with complete media at 37 °C under 5% CO_2.

Preparation of the *C. albicans* biofilm infected ECV 304 3D cell platform

A single colony of *C. albicans* was collected with a plastic loop and seeded in a 10 mL Yeast extract–Peptone–Dextrose (YPD) medium (Sigma-Aldrich, UK). The *C. albicans*–YPD suspension was incubated at 37 °C for 12 h with stirring at 150 rpm. The overnight culture (O/N) was centrifuged at 1000*g* for 5 min. The cell pellet was rinsed twice with sterile PBS solution to remove excess YPD medium before *C. albicans* were reseeded in RPMI medium supplemented with 1% L-glutamine. The fungal cell concentration was adjusted to 1×10^5 mL^{-1} by a series of dilutions using RPMI medium, since this is the optimal condition for the formation of the *C. albicans* biofilm. To monitor the spread of fungal infection, the *C. albicans* cells were stained using carboxyfluorescein succinimidyl ester (CFSE), which is a multi-generational dye that binds to lysine residues and other amine sources.[55] The CFSE dye has been employed to generationally track the bacterial proliferation over discrete cycles.[56] Extended research has demonstrated that CFSE was capable of monitoring the bacterial/human cell interaction.[57] CFSE shows green signals under a confocal microscope or a fluorescence microscope set at the FITC channel (494 nm). The protocol for staining the fungal cells is given below. Briefly, a 10 mL aliquot of the C. *albicans* suspension with a fixed cell concentration of 1×10^5 mL^{-1} was pelleted by centrifugation at 4000*g*. The sediment was rinsed twice with sterilized PBS solution and resuspended in 2 × CFSE working solution (20 μg CFSE in 10 ml PBS). The working suspension of *C. albicans* (labelled with CFSE or unlabeled) with an optimal cell density was seeded to the formed 3D ECV 304 cell clusteroid layer growing on the bottom of the six-well plates. Briefly, 20 μL of the *C. albicans* working suspension was added to each well. To allow the proliferation of the clusteroids, 200 μL DMEM complete medium was also pipetted into the wells. The plates were incubated at 37 °C for 12 h to generate a biofilm on the clusteroid layer. After the allotted time, the medium was discarded by gentle pipetting, and the clusteroids infected by the biofilm adhered to the wells were rinsed two times with sterilized PBS solution. DMEM medium was used for the cell culture and RPMI medium for the fungal cell culture.

Preparation of fluconazole-loaded P407-stabilised shellac NPs

To prepare the NP suspension, 200 μL of 25 wt% ammonium shellac solution (Aqua Gold) was diluted to 50 mL using deionized water to obtain 0.2 wt% ammonium shellac solution. Then 0.125 g of P407 and 0.01 g fluconazole were added to the 0.2 wt% shellac solution, followed by dropwise addition of 0.25 M NaOH to change the pH to 10. This was followed by 30 min sonication using an ultrasonic bath (Ultrawave, UK) at 40% of the maximum power of 200 at 25 °C, and 30 min of magnetic stirring was conducted to solubilize P407 and fluconazole. The pH was then adjusted to 5.5 using 0.25 M HCl solution to precipitate the individual components to shellac NPs.

The final concentration of the 1× stock NP formulation was 0.02 wt% fluconazole-loaded 0.2 wt% shellac NP sterically stabilized with 0.25 wt% P407.

Coating of the fluconazole-loaded shellac NPs with lysozyme

To functionalize the shellac nanoparticles with a cationic surface functionality, 0.125 g of lysozyme powder was added to the 0.02 wt% fluconazole-loaded 0.2 wt% shellac NPs stabilized with 0.25 wt% P407 with agitation. The solution was sonicated for 15 min to avoid aggregation. Lysozyme exhibits a very high positive charge at pH 5.5 and charge reverse the originally anionic shellac NPs into a cationic surface functionality by an electrostatic binding. The lysozyme-coated shellac NPs were collected by centrifugation at 8000*g* for 30 min. The pelleted NPs were then resuspended in 50 mL deionized water to reach a final concentration of 0.02 wt% fluconazole-loaded 0.2 wt% shellac NPs stabilized by 0.25 wt% P407 and coated with 0.2 wt% lysozyme. This concentration is treated as 1× stock suspension. To obtain a more concentrated 2×, 3×, or 4× suspension, the pelleted NPs were diluted in 25 mL, 16.7 mL, and 12.5 mL of deionized water, respectively.

Bright field, fluorescence, and confocal microscopy observations

The microstructure of the individual clusteroids and the proliferation of the clusteroids collected from the DEX/PEO emulsion template were imaged using a bright field optical microscope supplemented with a fluorescence microscope (Olympus BX-51). 20 μL of the sample was carefully pipetted onto a concave slide at room temperature under various immersion objectives. To visualize the clusteroids, 4′,6-diamidino-2-phenylindole (DAPI) was used as the fluorescence dye on the clusteroids before the clusteroids were observed. For tracking of the long-term proliferation of the clusteroids or *C. albicans*, CFSE was used, which would permeate into cells and bind to their interior by the succinimidyl group. The fungal and ECV 304 cells were pre-stained prior to the biofilm formation. For selective experiments, the clusteroids were stained using the

CellTracker Green CMFDA dye (5-chloromethylfluorescein diacetate) and *C. albicans* were stained with CFSE to allow monitoring over longer periods by fluorescence microscopy. The observation of the *C. albicans* biofilms and the 3D clusteroid co-culture model was carried out using a confocal laser scanning microscope (CLSM, Zeiss LSM710). Z-stack images were collected to generate a 3D view of the biofilms on the clusteroid model, which had 100 slices with 2 μm per slice. Two channels, 461 nm (DAPI) and 488 nm (FITC), were set at a precise mode to avoid signal interference of the fluorescence signal within the stained ECV 304 cell clusteroids and the *C. albicans* biofilm.

Biofilm clearance efficiency after the NP treatment

After the biofilm-infected ECV 304 *in vitro* 3D model was obtained by the method mentioned above, the culture was firstly rinsed with PBS twice to remove any remaining planktonic fungal cells. The 1× standard stock solution was 0.02 wt% fluconazole-loaded 0.2 wt% shellac NPs sterically stabilized with 0.25 wt% P407. 100 μL of 1×, 2×, 3× and 4× stock suspensions were added separately to the clusteroid/biofilm co-cultures and 100 μL of DMEM complete medium was supplemented to keep the cells proliferating. 0.1 mL of PBS with 0.2 mL DMEM complete medium was added to a well as the control. The antibiofilm properties of the individual components of the NPs were also tested to prove the efficiency of the nanostructure. 100 μL of the prepared solutions of different individual components with an equal concentration in the NPs were also added into different well plates containing the biofilm/ECV 304 clusteroid co-cultures. After 24 h of treatment, the media were discarded, and the cultures were collected and shaken for 30 s with glass beads to release the fungal cells from the biofilm. The samples were then transferred to test tubes with 100 μL of fresh Mueller–Hinton broth (MHB). Each example was vortexed for 30 s to disassociate the biofilm and inoculate the MHB with fungal cells. The drop plate count technique was utilized to quantify cell colony forming unit (CFU) per mL. To enumerate the fungal cell viability inside the biofilms, 10× dilutions were made in the MHB and 10 μL solutions were transferred onto the MHA plates and

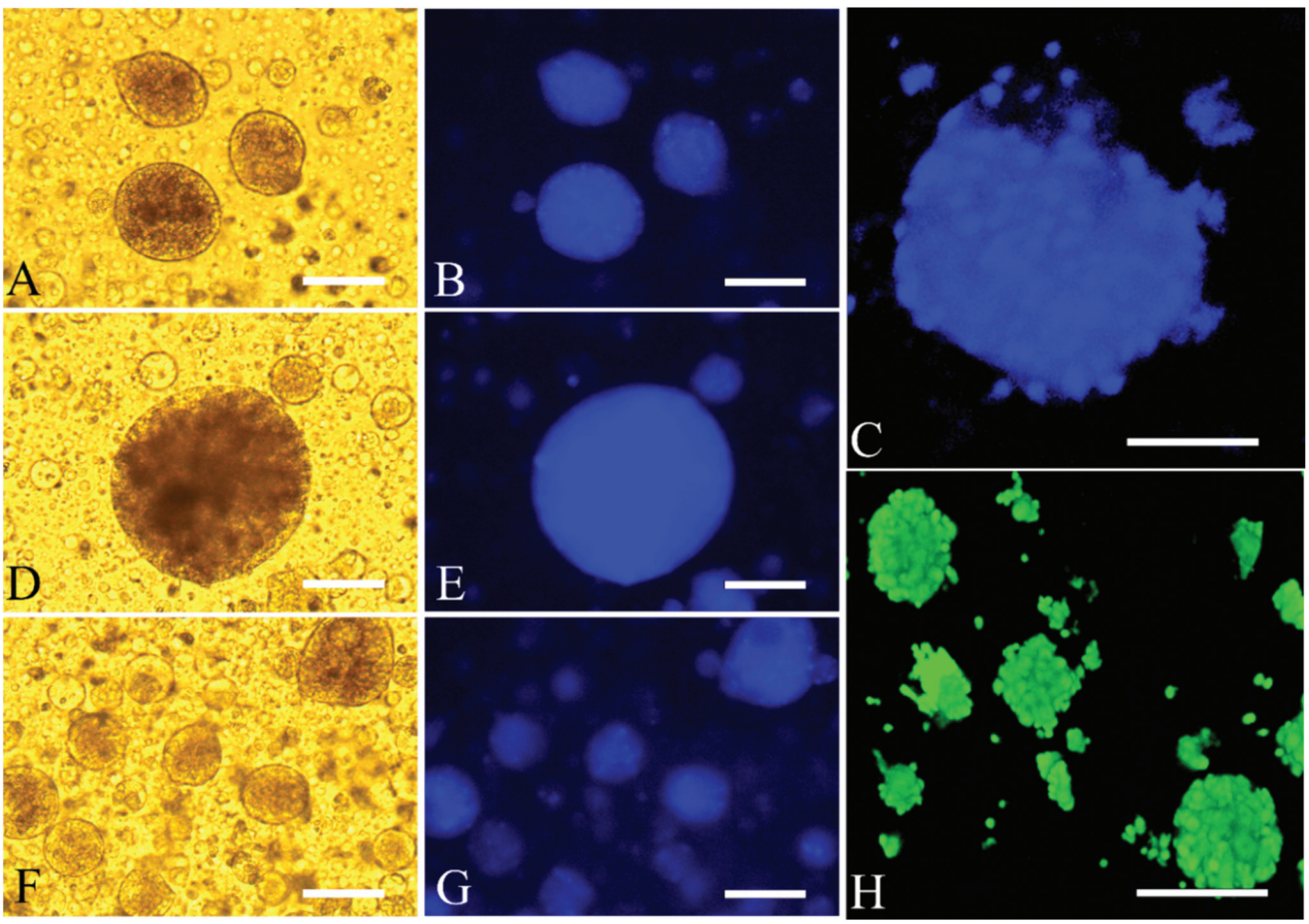

Fig. 2 Optical bright field microscopy images (A, D and F), fluorescence microscopy images (B, E, G and C), and confocal laser scanning microscopy observation (E) of the individual ECV 304 cell clusteroids encapsulated in the w/w Pickering emulsions (5.5 wt% DEX and 5.5 wt% PEO).[36,37] The clusteroids were stained with DAPI (B, E, G and C) or FDA live/dead assay (H). The scale bar is 50 μm for (A, B, D and E), 100 μm for (F and G), 50 μm for (C) and 200 μm for (H). The fluorescence intensity was measured using ZEN software (blue edition).

left growing for 24 hours at 37 °C. The CFUs were checked from the last two droplets, which contained a countable number of CFUs (3 to 30 counts for every 10 μL drop) and the average count was calculated. Compared to the conventional CFU assay, the drop plate count technique (10 μL drop) allowed us to count the visible colonies faster and more accurately by distributing the samples in drops.[54]

Cytotoxicity test of the NP treatment using an MTS assay

The cytotoxicity of the NP treatment on the ECV 304 cell clusteroids is a key feature in evaluating their potential to be used in clinical applications. An MTS assay was used to test the ECV 304 cell viability after the clusteroids were exposed to the NP treatment. The MTS assay evaluated the cell metabolic activity. Nicotinamide adenine dinucleotide phosphate (NADPH)-dependent cellular oxidoreductase enzymes may, under defined conditions, reflect the number of viable cells present. These enzymes can reduce the tetrazolium dye, 3-(4,5-dimethylthiazol-2-yl)-5-(3-carboxymethoxyphenyl)-2-(4-sulfophenyl)-2H-tetrazolium (Compound 1), to a soluble formazan product. 20 μL of the MTS compound was added to each microwell containing ECV 304 cell clusteroids with an initial cell number of about 5×10^5, supplemented with 100 μL DMEM complete medium, after 1 h and 48 h of cell incubation at 37° C under 5% CO_2, respectively. The microwell plates were then incubated for another 30 min and then their absorbance at 490 nm was measured using a microplate reader (BioTek Synergy HT).

SEM imaging of shellac NPs, ECV 304 cells, and *C. albicans* biofilms on the ECV 304 3D clusteroid layer

A sample of the stock formulation of 0.02 wt% fluconazole-loaded 0.2 wt% shellac NPs stabilized by 0.25 wt% P407 and coated with 0.2 wt% lysozyme was left to air-dry before it was coated with gold for imaging. ECV 304 cells, *C. albicans* biofilm infected clusteroids, and NPs treated clusteroid/biofilm co-culture were gently collected from the well plate using a sterilized loop and shifted to glass slides. The cultures were fixed with 1 wt% glutaraldehyde in PBS buffer solution for 1 h at 25 °C. The cultures were then rinsed three times with deionized water to wash away excess glutaraldehyde. Post treatment, the 3D clusteroids were gently removed from the plate using a sterilised loop and placed onto a 7 mm diameter circular glass slide and adhered to carbon discs. The biofilm was gently washed with deionized water to remove the excess media and NPs. The biofilms were then fixed with 1 wt% glutaraldehyde in PBS buffer solution for 1 h at room temperature. After fixation, the biofilms were washed 3 times with deionized water to remove excess glutaraldehyde. Samples were imaged using Zeiss SmartSEM software (Zeiss Evo-60 S.E.M., Germany). The SEM images were processed with a pseudo-color to distinguish cells from the biofilms (yellow colour for the cells and green for the *C. albicans* biofilm).

Cryostat sectioning

For the characterization of the fungal infection inside the clusteroid layer, the *C. albicans* infected layer of the ECV 304 clus-

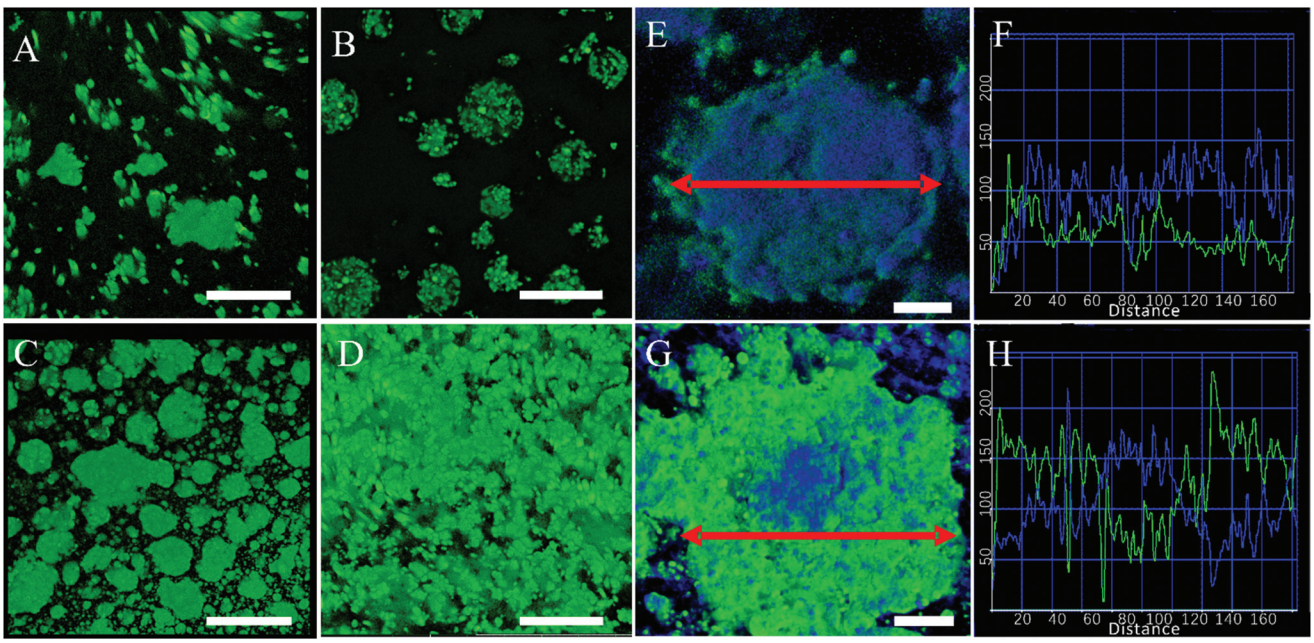

Fig. 3 CLSM images of the proliferation of the clusteroid layer at different days of culture: (A) day 1; (B) day 3; (C) day 5; and (D) day 7. The initial cell number was normalized to 1 × 106 cells per mL. Zeiss LSM750 fluorescence microscope was employed to capture the images. The scale bar is 100 μm for the confocal laser scanning microscopy observation of individual ECV 304 clusteroids infected by *C. albicans* after (E) 1 h and (G) 24 h. The graphs in (F) and (H) show the fluorescence intensity of (A) and (C), respectively. The scale bar is 50 μm. The red arrows indicate the lines along which the fluorescence intensity was measured.

teroid culture was detached from the microwell plate by a sterilized loop and placed on filter paper. The culture was then frozen in optimal cutting temperature (OTC) compound overnight before cryostat sectioning. A Leica CM1950 was used to create slices with a thickness of 10 μm, and the slice in the central region was collected and moved onto the glass slide. An Olympus BX51 fluorescence microscope was used to visualize the sectioned slices.

Results and discussion

Preparation of the ECV 304 clusteroids and the 3D clusteroid layer

The ECV 304 cells were harvested after the 2D cell monolayer culture reached 80% confluency, after which they were moved to the DEX/PEO w/w Pickering emulsion template stabilized by 2 wt% whey protein particles. The cells were compacted in the droplets by adding a PEO solution of a higher concentration. The shrinking process would provide increased cell–cell adhesion and induce the formation of clusteroids (Fig. S1, ESI†). Notably, the concentration of PEO/DEX and the shrinking process are essential in clusteroid formation, which was proved in our former works.[27,36–38] The clusteroids were left in the w/w Pickering emulsion for 12 h to allow cell interaction and adherence, after which they were collected by diluting the emulsion 10-fold with PBS, Fig. S1 (ESI).† Typical ECV 304 clusteroids collected from the w/w emulsions are shown in Fig. S2.† The SEM images compared the individual ECV 304 cells (Fig. S2A, ESI†) with the clusteroids of ECV 304 cells (Fig. S2B, ESI†), which clearly shows the microstructure of the cells within. The collected clusteroids were stained with DAPI and treated with FDA to preliminarily assess their integrity and cell viability (Fig. 2). We found that the clusteroid formation process, which is based on the ATPS,[27,36–38] did not adversely impact the viability of the cells in the clusteroids, as shown in Fig. S3.† A fixed number of cells (1×10^5 mL^{-1}) were formulated as clusteroids and then were moved to 96 microwell plates precoated with poly-L-lysine. This substrate allows the formation of a clusteroid layer on the bottom of the wells. The growth of the clusteroids was continually monitored by CMFDA cell labelling (a generational dye for living cell tracking). As shown in the images in Fig. 3A–G and S4,† this indicates that the clusteroids would proliferate rapidly and fuse into a dense 3D clusteroid layer, which could potentially work as a proxy for the bladder's inner layer of urothelial cells within 7 days. The individual clusteroids grew and they percolated with each other and started fusing into a tissue-like 3D compacted layer.

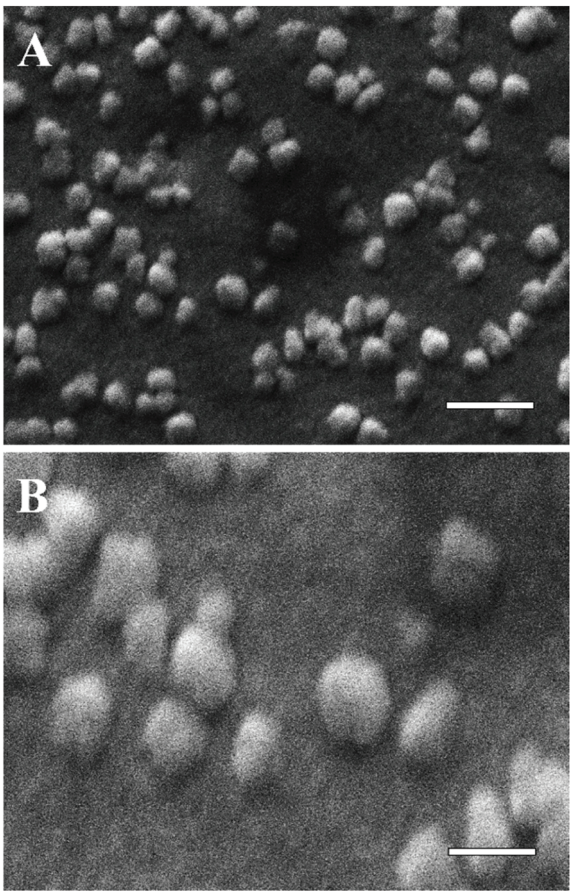

Fig. 4 SEM observation of 0.25 wt% P407-stabilized 0.02 wt% fluconazole-loaded 0.2 wt% lysozyme coated 0.2 wt% shellac nanoparticles. The scale bar is 500 μm for (A) and 100 μm for (B).

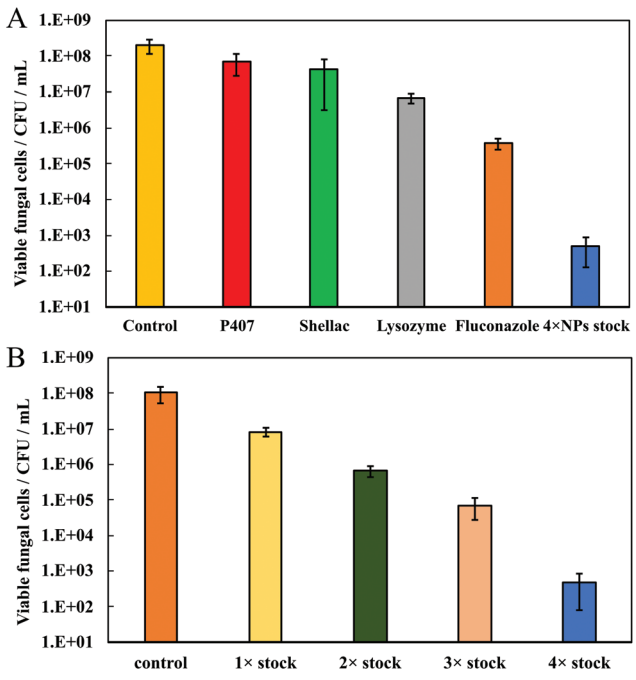

Fig. 5 (A) Efficiency of equivalent individual components of the 4× stock NP solution on the clearance of the *C. albicans* biofilm infected on the 3D culture of the ECV 304 cell clusteroid layer. The fungal cell numbers were normalized by CFUs. (B) Influence of different concentrations of the lysozyme-coated fluconazole-loaded shellac NPs on the proliferation of the 3D culture of the ECV 304 clusteroid layer after 1 h and 48 h. The concentration of the 1× standard stock solution is 0.2 wt% shellac, 0.25 wt% P407, 0.2 wt% lysozyme and 0.02 wt% fluconazole.

The fusion of the clusteroids is shown in Fig. S4.† Overall, these results indicate that our w/w Pickering emulsion template would be an ideal platform for the fast preparation of such a realistic *in vitro* environment which can be further explored after biofilm infection and treatment.

C. albicans infection and the formation of a biofilm on top of the ECV 304 3D clusteroid layer

The purpose here was to determine the biofilm formation on our simulated bladder inner urothelial wall model. The biofilm formation mechanism on implanted devices and the surface of various substrates has been well established and studied,[39,40] including tissues and implanted devices.[41–45] Our previous work has successfully demonstrated the *S. aureus* and *P. aeruginosa* biofilm formation on keratinocyte clusteroids.[27] The formation of biofilm on an *in vitro* bladder wall model has not yet been explored up to the best of our knowledge. To assess the biofilm-infected 3D clusteroid layer model, a confocal microscopy observation was employed to confirm that *C. albicans* could successfully embed on the 3D clusteroid layer (Fig. 3E–H).

The invasion of the fungal cells into individual cell clusteroids is clearly shown in Fig. 3E and G. After 1 h of incubation, the fungal cells started to proliferate and surround the ECV 304 clusteroids. The difference between the "1 h" and "24 h" groups was clear; the fluorescence signals were dominated by the green FITC channel, which indicates the coverage of fungal cells on the layer of clusteroids and the formation of a biofilm. Similarly, the build-up of a *C. albicans* biofilm above the 3D clusteroid layer was also investigated using CLSM (Fig. 3F and H). After 24 h, one can also observe the biofilm generation on the clusteroid layer, which correlates with the results of fluorescence microscopy. The specific morphology of the *C. albicans* biofilm on the ECV 304 cell clusteroids and the 3D clusteroid layer was further observed using SEM. As shown in Fig. S2A and S2B,† the individual *C. albicans* cells have an oval shape and

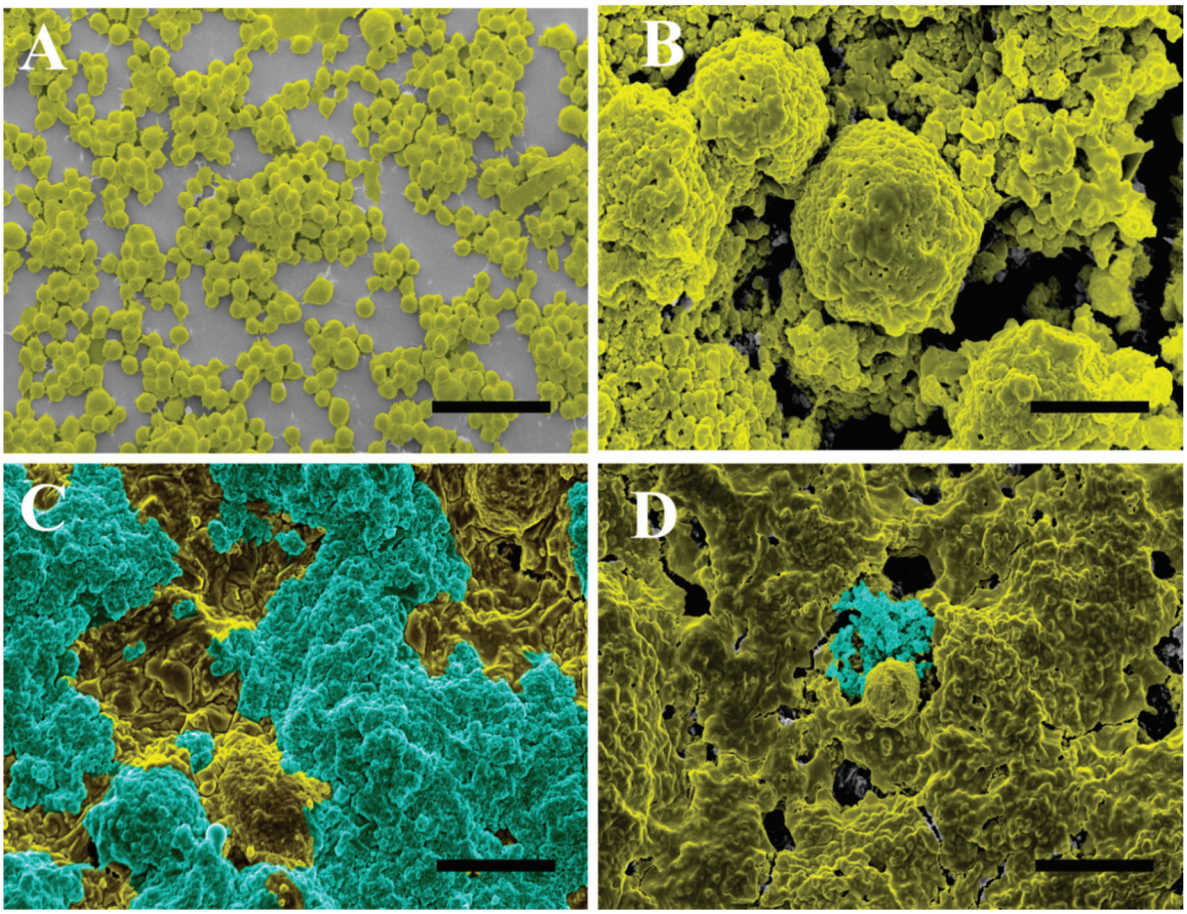

Fig. 6 Pseudo colour SEM images of (A) a layer of individual ECV 304 cells without any fungal infection or treatment by 4× lysozyme-coated fluconazole-loaded shellac NP stock solution. (B) Individual ECV 304 clusteroid layer without fungal infection or lysozyme-coated fluconazole-loaded shellac NP treatment. (C) ECV 304 clusteroid layer infected with the *Candida albicans* biofilm. (D) The ECV 304 clusteroid layer infected with the *C. albicans* biofilm imposed by the treatment of lysozyme-coated fluconazole-loaded shellac NP stock formulation. The scale bar is 100 μm for (A–C) and 200 μm for (D). The 1× stock suspension of the lysozyme-coated fluconazole-loaded shellac NPs is 0.2 wt% shellac, 0.25 wt% P407, 0.2 wt% lysozyme and 0.02 wt% fluconazole. The cell concentration used in the experiments was 1×10^5 mL^{-1}. Yellow colour represents the ECV 304 cell clusteroids, while green colour represents the *C. albicans* biofilm. The original SEM images are shown in Fig. S2.†

produce a thick aggregated layer on top of the ECV 304 clusteroids. Note that the formation of the biofilm does not disintegrate the structure of the layer of cell clusteroids.

Characterization of the lysosome-coated fluconazole-loaded shellac NPs

Detailed characterisation results of the fluconazole nanocarrier are presented in the ESI.† The results obtained from the average hydrodynamic diameter and zeta-potential analysis of the produced shellac NPs as a function of fluconazole concentration at pH 5.5 are shown in Fig. S5B.† The increase of the fluconazole concentration had only a very minor effect on the average nanoparticle hydrodynamic diameter, ranging between 68 nm and 79 nm, Fig. S5A.† As can be seen from Fig. S5E,† the pH had only a minor effect on the fluconazole encapsulation efficiency. All the set groups yielded an encapsulation efficiency higher than 70%. The release kinetics of fluconazole from the 1× stock suspension of NPs was measured at pH 5.5 as a function of time. Fig. S5F† shows that fluconazole was released to about 50% after 15 h and approximately 70% after 25 h. Such release kinetics makes the nanocarrier suitable for treating the biofilms. The size of the nanoparticles shown in the SEM images (Fig. 4) correlated with the results obtained from the Zetasizer measurements (Fig. S5A and C – ESI†). The NPs had a spherical shape and were about 60–90 nm in size. The zeta-potential was influenced by fluconazole with no more than 30% variation (Fig. S5B – ESI†). The negative surface charging remained in all the set groups due to the residual –COOH groups of the shellac components (shellolic acids).

The efficiency of the lysozyme-coated fluconazole-loaded NP treatment for the clearance of the *Candida albicans* biofilm on the 3D layer of the ECV 304 cell clusteroids

Here we examined the antifungal activity of the lysozyme-coated shellac nanocarriers of fluconazole on the biofilm

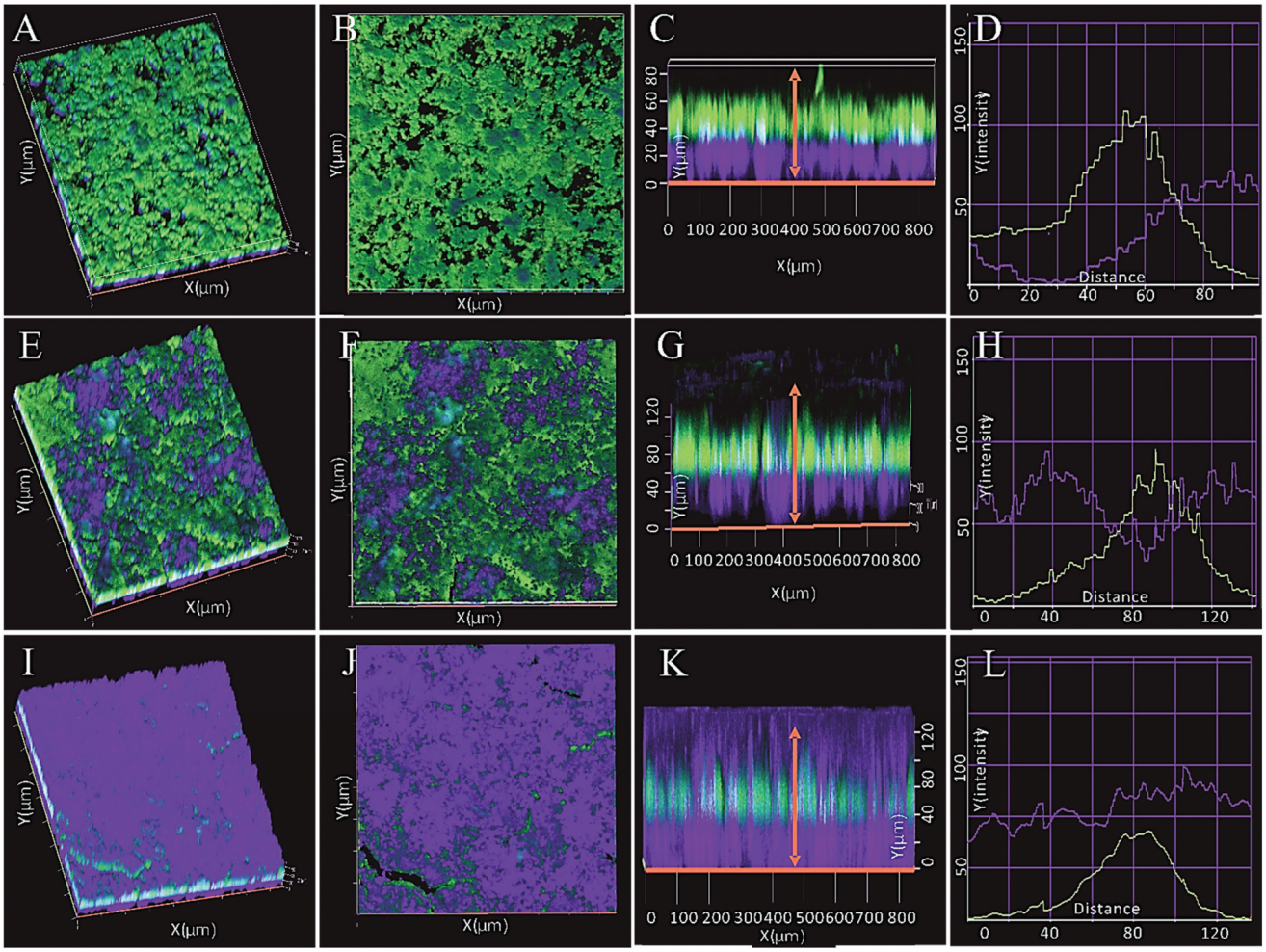

Fig. 7 Confocal laser scanning microscopy observation of the biofilm/ECV 304 clusteroid co-cultures before (A–C) and after 12 h (E–G) and 24 h (I–K) of the treatment of 4× stock solution of the NPs. The scale bar is 50 μm for D–J. The fluorescence intensity of the figures C, G and K is displayed in figures D, H and L, respectively. The size of the box is 800 μm × 800 μm × 80 μm (*X*, *Y* and *Z*). The concentration of the 1× stock solution of NPs is 0.2 wt% shellac, 0.25 wt% P407, 0.2 wt% lysozyme and 0.02 wt% fluconazole. The fluorescence intensity was measured using ZEN software (blue edition). The red arrows indicate where the fluorescence intensity was measured.

anchored on the 3D layer of urothelial clusteroids. To determine the efficiency of the biofilm clearance of the NPs, different concentrations of stock solutions were applied on the *C. albicans* biofilm infected 3D layer of the ECV 304 cell clusteroids.

As can be seen in Fig. 5A, the increased concentration of the NPs delivered higher efficiency on clearance of the fungal biofilm, with a 5-log reduction on the overall amount of the viable fungal cells when treated with 4× stock solution of the NPs. A lower NP concentration was not enough to clear the whole fungal biofilm. This could be attributed to the intrinsic and high resistance of *C. albicans* to fluconazole. The individual components of the NPs were also separately tested for their efficiency of biofilm clearance with an equal concentration to the formulation used in the NPs. Fig. 5B shows that the major contributor to the antifungal action was brought by the fluconazole payload. Lysozyme also showed a certain fungal killing effect, as it can catalyze the hydrolysis of 1,4-beta-linkages between *N*-acetylmuramic acid and *N*-acetyl-D-glucosamine residues in peptidoglycans. The other components of the NPs showed very limited positive effects on biofilm clearance.

SEM imaging was employed to examine the microstructure of the fungal biofilm infection on the 3D layer of clusteroids (Fig. 6). The biofilm was manually adjusted to green colour, and the cells yellow. The SEM images clearly show the morphology of the biofilm stuck on the cell clusteroid layer (Fig. 6C and D). After the treatment of the NPs, only a few planktonic fungal cells could be observed. The original images of SEM are provided in Fig. S2 (ESI).†

It is worth mentioning that none of the individual components of the nanocarrier could match the biofilm clearing efficiency of the composite NPs, which dominated the effect of the individual components. These results indicate the synergistic effect of the nano-formulation in killing the *C. albicans* cells and clearing the fungal biofilm. To illustrate the biofilm removal, the biofilm clearing process of the 4× stock NPs solution was visualized using CLSM observations. The 3D layer of clusteroids was pre-stained with DAPI dye before the fungal biofilm infection, which was contrast-stained with CFSE.

The removal of the biofilm was partly achieved after 1 h of incubation starting from the outer layer of the biofilm (Fig. 7A–D). The CFSE fluorescence signal was slightly reduced. After 12 h of incubation with the NP treatment, half of the biofilm deposited on the surface of the clusteroids peeled off (Fig. 7E–H). After 24 h incubation, the biofilm initially attached to the surface of the 3D clusteroid layer was mostly removed, only leaving a very low number of fungal cells inside of the clusteroid layer (Fig. 7H–K). This could be proven by the fluorescence intensity, which showed that the signals peaked at the central area. The intractability of the complete removal of the biofilm is mainly derived from its thick EPS. The long-term release and the electrostatic absorbance of the NPs showed a positive synergistic effect on clearing the biofilm. However, the images collected from CLSM observations demonstrated that the partly rough morphology of the 3D layer of clusteroids may potentially reduce the efficiency of the fungal biofilm removal. To clarify this point, cryostat sectioning was used to visualize whether the fungal cell infection

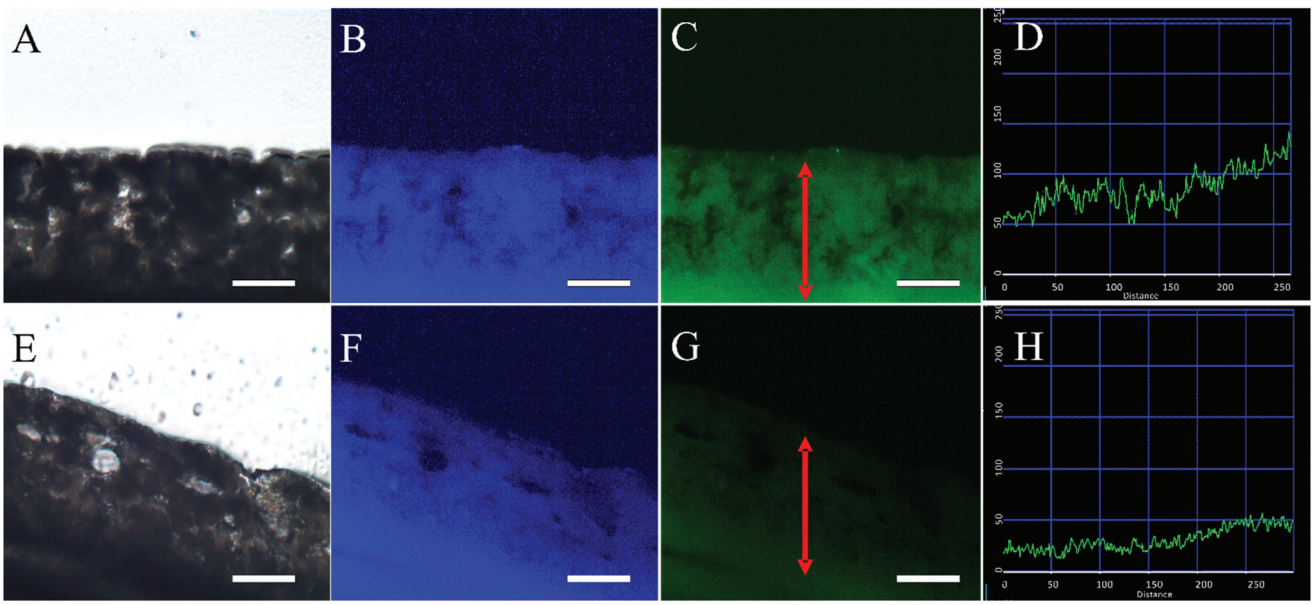

Fig. 8 Microscopy observation of the cryostat sectioned slices of the 3D co-cultured fungal biofilm infected clusteroid layer: before (A–C) and after (E–G) treatment with 4× stock solution. Each slice produced by the cryosectioning is 10 μm. An Olympus BX51 fluorescence microscope was used for the series of observations. The fluorescence intensity of C and G was measured using ZEN software (blue edition), and is shown in D and H, respectively. The scale bar is 100 μm (same for all images). The concentration of 1× stock suspension is 0.2 wt% shellac, 0.25 wt% P407, 0.2 wt% lysozyme and 0.02 wt% fluconazole. The red arrows indicate where the fluorescence intensity was measured.

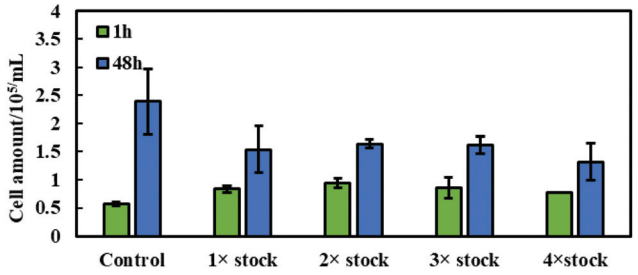

Fig. 9 Cytotoxicity of different concentrations of lysozyme-coated fluconazole-loaded shellac NPs suspensions on the proliferation of the 3D layers of ECV 304 clusteroids after 1 h and 48 h of culture. The cell numbers in the different cultures taken after 1 h and 48 h were calculated using the standard curve.

in the core of the clusteroids was restrained. Fig. 8 shows the junction of the clusteroids in the bright field observations. Similarly, the green fluorescence signal from the fungal cells was reduced by over 60%. However, a minor residue of fungal cells could still be detected in the sectioned slice after the 4× stock solution treatment.

Cytotoxicity of the NPs treatment on the ECV 304 clusteroids

Different concentrations of NPs stock suspensions were added to the microwell plate containing the 3D cell clusteroid layer to investigate the cytotoxicity of the NPs on the ECV 304 cells. In clinical practice, the utilization of the NPs treatment would potentially affect the surrounding uninfected cells. To evaluate and potentially reduce this influence, the cytotoxicity test was carried out using an MTS assay. Fig. 9 shows that 1× stock solution could reduce the overall cell amount by 40% after 48 h. Interestingly, the cell proliferation was not impaired by the addition of a highly concentrated amount of NPs (4× stock), which indicates a saturation. The 4× stock solution had only a negligible effect on the ECV 304 cell viability. No significant difference was observed in the ECV 304 cell amount after 1 h of treatment with different concentrations of the stock solution. Compared to the 5-log reduction in the *C. albicans* cells after 24 h of treatment, only a 40% inhibition on ECV 304 cell proliferation clearly indicated this NP treatment as an efficient biofilm cleaning formulation.

Conclusions

Here we developed a *C. albicans* biofilm-infected 3D urothelial cell clusteroid model for mimicking the bladder inner cell wall. For clearing fungal biofilms on the 3D layer of urothelial clusteroids, we designed a fluconazole-loaded shellac nanotherapeutic system using a coating of the cationic enzyme lysozyme to functionalize the fluconazole nanocarriers. The cationic lysozyme coating reversed the surface charge and changed the negatively charged shellac NPs into positively charged nanocarriers targeting the negatively charged *C. albicans* biofilm. The idea is that the lysozyme-coating of the nanocarrier would partially digest the EPS of the biofilm which is rich in peptidoglycans and facilitate the delivery of the antifungal agent fluconazole to the encased *C. albicans* cells.

CLSM and SEM imaging, bright field microscopy, CFU counts, MTS assay, and cryostat sectioning were employed to characterise the state of the *C. albicans* biofilm infected 3D layer of the urothelial clusteroids before and after the nanotherapy treatment. These antifungal NPs showed a significant enhancement of the biofilm clearing effect compared to any free individual components (shellac, P407, or fluconazole). The strong antifungal effect of this treatment did not significantly increase the cytotoxicity of the 3D clusteroid model; the treatment of the clusteroids brought minor effects on the clusteroid proliferation. The whole process of this work includes urothelial cell culture and formation of cell clusteroids, biofilm infection, and NP treatment. Such a protocol could be potentially used as a general platform for mimicking a wide range of fungal biofilm infections or bacterial infections on selected organs or body parts by replacing the species of cell type and pathogen type. Taken together, the introduced biofilm-infected 3D urothelial cell clusteroid platform is an ideal model for mimicking urinary tract infection. This platform provides researchers with a facile approach for testing various therapeutics, especially nanocarrier-based therapeutics, for biofilm clearance. This work would fill in the gaps in *in vitro* urinary models for biofilm infection and could be a useful guide for relevant biofilm *in vitro* simulations which are expected to facilitate the clinical use of nanotechnology-based antimicrobial therapeutics.

Author contributions

A. W.: methodology, investigation, formal analysis, data curation, writing – original draft, and writing – review and editing. P. J. W.: methodology, investigation, data curation, and writing – review and editing. L. A. M.: investigation, methodology, supervision, and writing – review and editing. V. N. P.: conceptualization, methodology, supervision, and writing – review and editing. All authors have read and agreed to the published version of the manuscript.

Conflicts of interest

There are no conflicts to declare.

Acknowledgements

A. W. thanks the Chinese Scholarship Council for the financial support of his Ph.D. studies. The authors would like to thank the SEM technician Mr Timothy Dunstan (The University of Hull) for his assistance during this project.

References

1 J. Kaufman, M. Temple-Smith and L. Sanci, *BMJ Paediatr. Open*, 2019, **3**, e000487.
2 P. Yousefi, A. Cyrus, Z. Moghaddasi, F. Dorreh and A. Aravand, *J. Adv. Med. Biomed. Res.*, 2011, **19**, 66–76.
3 K. Gupta, L. Grigoryan and B. Trautner, *Ann. Intern. Med.*, 2017, **167**, ITC49–ITC64.
4 T. M. Hooton, *J. Antimicrob. Chemother.*, 2000, **46**(Suppl 1), 1–7; discussion 63–5.
5 K. Gupta, T. M. Hooton, K. G. Naber, B. Wullt, R. Colgan, L. G. Miller, G. J. Moran, L. E. Nicolle, R. Raz, A. J. Schaeffer and D. E. Soper, *Clin. Infect. Dis.*, 2011, **52**, e103–e120.
6 C. W. Tan and M. P. Chlebicki, *Singapore Med. J.*, 2016, **57**, 485–490.
7 F. Wagenlehner and K. Naber, *J. Hosp. Infect.*, 2000, **46**, 171–181.
8 J. R. Phillips and M. G. Karlowicz, *Pediatr. Infect. Dis. J.*, 1997, **16**, 190–194.
9 E. H. Elpern, K. Killeen, A. Ketchem, A. Wiley, G. Patel and O. Lateef, *Am. J. Crit. Care*, 2009, **18**, 535–541; quiz 542.
10 S. Niveditha, S. Pramodhini, S. Umadevi, S. Kumar and S. Stephen, *J. Clin. Diagn. Res.*, 2012, **6**, 1478–1482.
11 H. Pelling, J. Nzakizwanayo, S. Milo, E. L. Denham, W. M. MacFarlane, L. J. Bock, J. M. Sutton and B. V. Jones, *Lett. Appl. Microbiol.*, 2019, **68**, 277–293.
12 N. S. Morris, D. J. Stickler and R. J. McLean, *World J. Urol.*, 1999, **17**, 345–350.
13 S. P. Hawser and L. J. Douglas, *Infect. Immun.*, 1994, **62**, 915–921.
14 J. Chandra, D. M. Kuhn, P. K. Mukherjee, L. L. Hoyer, T. McCormick and M. A. Ghannoum, *J. Bacteriol.*, 2001, **183**, 5385–5394.
15 D. Davies, *Nat. Rev. Drug Discovery*, 2003, **2**, 114–122.
16 G. O'Toole, H. B. Kaplan and R. Kolter, *Annu. Rev. Microbiol.*, 2000, **54**, 49–79.
17 M. G. Trulear and W. G. Characklis, *J. – Water Pollut. Control Fed.*, 1982, **54**, 1288–1301.
18 K. Lewis, *Antimicrob. Agents Chemother.*, 2001, **45**, 999–1007.
19 H.-C. Flemming and J. Wingender, *Nat. Rev. Microbiol.*, 2010, **8**, 623–633.
20 L. Robino and P. Scavone, *Future Microbiol.*, 2020, **15**, 377–379.
21 Y. Liu, L. Shi, L. Su, H. C. van der Mei, P. C. Jutte, Y. Ren and H. J. Busscher, *Chem. Soc. Rev.*, 2019, **48**, 428–446.
22 E. N. Taylor, K. M. Kummer, D. Dyondi, T. J. Webster and R. Banerjee, *Nanoscale*, 2014, **6**, 825–832.
23 F. Haghighi, S. R. Mohammadi, P. Mohammadi, M. Eskandari and S. Hosseinkhani, *Bratisl. Lek. Listy*, 2012, **113**, 707–711.
24 S. M. Abdelghany, D. J. Quinn, R. J. Ingram, B. F. Gilmore, R. F. Donnelly, C. C. Taggart and C. J. Scott, *Int. J. Nanomed.*, 2012, **7**, 4053–4063.
25 K. Qvortrup, L. D. Hultqvist, M. Nilsson, T. H. Jakobsen, C. U. Jansen, J. Uhd, J. B. Andersen, T. E. Nielsen, M. Givskov and T. Tolker-Nielsen, *Front. Chem.*, 2019, **7**, 742.
26 P. J. Weldrick, M. J. Hardman and V. N. Paunov, *Mater. Chem. Front.*, 2021, **5**, 961–972.
27 A. Wang, P. J. Weldrick, L. A. Madden and V. N. Paunov, *ACS Appl. Mater. Interfaces*, 2021, **13**, 22182–22194.
28 P. J. Weldrick, M. J. Hardman and V. N. Paunov, *ACS Appl. Mater. Interfaces*, 2019, **11**, 43902–43919.
29 A. F. Halbus, T. S. Horozov and V. N. Paunov, *ACS Appl. Mater. Interfaces*, 2019, **11**, 12232–12243.
30 P. J. Weldrick, S. Iveson, M. J. Hardman and V. N. Paunov, *Nanoscale*, 2019, **11**, 10472–10485.
31 D. Huh, G. A. Hamilton and D. E. Ingber, *Trends Cell Biol.*, 2011, **21**, 745–754.
32 M. Ravi, V. Paramesh, S. R. Kaviya, E. Anuradha and F. D. P. Solomon, *J. Cell. Physiol.*, 2015, **230**, 16–26.
33 O. Chaudhuri, *Biomater. Sci.*, 2017, **5**, 1480–1490.
34 V. van Duinen, S. J. Trietsch, J. Joore, P. Vulto and T. Hankemeier, *Curr. Opin. Biotechnol.*, 2015, **35**, 118–126.
35 A. Wang, L. A. Madden and V. N. Paunov, *J. Mater. Chem. B*, 2020, **8**, 10487–10501.
36 A. A. K. Das, B. W. Filby, D. A. Geddes, D. Legrande and V. N. Paunov, *Mater. Horiz.*, 2017, **4**, 1196–1200.
37 S. B. G. Celik, S. R. Dominici, B. W. Filby, A. A. K. Das, L. A. Madden and V. N. Paunov, *Biomimetics*, 2019, **4**, 50.
38 A. Wang, L. A. Madden and V. N. Paunov, *Mater. Adv.*, 2020, **1**, 3022–3032.
39 Z. Khatoon, C. D. McTiernan, E. J. Suuronen, T.-F. Mah and E. I. Alarcon, *Heliyon*, 2018, **4**, e01067.
40 S. Veerachamy, T. Yarlagadda, G. Manivasagam and P. K. Yarlagadda, *Proc. Inst. Mech. Eng., Part H*, 2014, **228**, 1083–1099.
41 W. Fu, T. Forster, O. Mayer, J. J. Curtin, S. M. Lehman and R. M. Donlan, *Antimicrob. Agents Chemother.*, 2010, **54**, 397–404.
42 A. E. Hodgson, S. M. Nelson, M. R. W. Brown and P. Gilbert, *J. Appl. Bacteriol.*, 1995, **79**, 87–93.
43 K. Marion-Ferey, M. Pasmore, P. Stoodley, S. Wilson, G. P. Husson and J. W. Costerton, *J. Hosp. Infect.*, 2003, **53**, 64–71.
44 C. Badet, A. Furiga and N. Thébaud, *Oral Health Prev. Dent.*, 2008, **6**, 337–341.
45 K. E. Hill, S. Malic, R. McKee, T. Rennison, K. G. Harding, D. W. Williams and D. W. Thomas, *J. Antimicrob. Chemother.*, 2010, **65**, 1195–1206.
46 S. S. M. Al-Obaidy, G. M. Greenway and V. N. Paunov, *Nanoscale Adv.*, 2019, **1**, 858–872.
47 S. S. M. Al-Obaidy, A. F. Halbus, G. M. Greenway and V. N. Paunov, *J. Mater. Chem. B*, 2019, **7**, 3119–3133.
48 A. P. Richter, J. S. Brown, B. Bharti, A. Wang, S. Gangwal, K. Houck, E. A. Cohen Hubal, V. N. Paunov, S. D. Stoyanov

and O. D. Velev, *Nat. Nanotechnol.*, 2015, **10**, 817–823.
49 M. J. Al-Awady, A. Fauchet, G. M. Greenway and V. N. Paunov, *J. Mater. Chem. B*, 2017, **5**, 7885–7897.
50 M. Al-Awady, P. J. Weldrick, M. J. Hardman, G. M. Greenway and V. N. Paunov, *Mater. Chem. Front.*, 2018, **2**, 2032–2044.
51 A. F. Halbus, T. S. Horozov and V. N. Paunov, *Biomimetics*, 2019, **4**, 1–20.
52 A. F. Halbus, T. S. Horozov and V. N. Paunov, *Nanoscale Adv.*, 2019, **1**, 2323–2336.
53 M. J. Al-Awady, G. M. Greenway and V. N. Paunov, *RSC Adv.*, 2015, **5**, 37044–37059.
54 B. Herigstad, M. Hamilton and J. Heersink, *J. Microbiol. Methods*, 2001, **44**, 121–129.
55 C R. Parish, *Immunol. Cell Biol.*, 1999, **77**, 499–508.
56 H. Tuominen-Gustafsson, M. Penttinen, J. Hytönen and M. K. Viljanen, *BMC Microbiol.*, 2006, **6**, 92.
57 D. Hoefel, W. L. Grooby, P. T. Monis, S. Andrews and C. P. Saint, *J. Microbiol. Methods*, 2003, **52**, 379–388.
58 P. J. Weldrick, M. J. Hardman and V. N. Paunov, *Adv. Nanobiomed. Res.*, 2021, **1**, 2000027.